Standing Self-Manipulation for a Legged Robot

Aaron M. Johnson[*], G. Clark Haynes[†], and D. E. Koditschek[*]

Abstract— On challenging, uneven terrain a legged robot's open loop posture will almost inevitably be inefficient, due to uncoordinated support of gravitational loads with coupled internal torques. By reasoning about certain structural properties governing the infinitesimal kinematics of the closed chains arising from a typical stance, we have developed a computationally trivial self-manipulation behavior that can minimize both internal and external torques absent any terrain information. The key to this behavior is a change of basis in torque space that approximates the partially decoupled nature of the two types of disturbances. The new coordinates reveal how to use actuator current measurements as proprioceptive sensors for the approximate gradients of both the internal and external task potential fields, without recourse to further modeling. The behavior is derived using a manipulation framework informed by the dual relationship between a legged robot and a multifingered hand. We implement the reactive posture controller resulting from simple online descent along these proprioceptively sensed gradients on the X-RHex robot to document the significant savings in standing power.

I. INTRODUCTION

In this paper we document a quasi-static RHex [1], controller that delivers up to a 90% improvement in power efficiency relative to the original open loop scheme for stand-in-place tasks on unmodeled rough terrain. The scheme is extraordinarily simple: the controller seeks simultaneously to reduce the variance of joint torques around their mean, while fighting to "lean up" against the mean load. The left side of Figure 1 depicts a configuration where the legs are producing equal torque, and so the robot must shift uphill to reduce this mean torque. The right side depicts a configuration where the average torque is zero, but the robot must relax its motors to reduce the variance. Formalizing these insights, we exploit the duality between a multi-fingered grasp and a multi-legged stance to establish the correctness of the controller by a quasi-static analysis borrowed from the robot manipulation literature, following [2]. Finally, after presenting data from this "reactive stand" behavior, implemented on the X-RHex robot [3], we offer a preliminary extension of the standing controller into a walking domain that achieves a 30%- 40% decrease in peak thermal loading.

This notion of fighting an external force and relaxing the internal force has been used before on legged robots, usually without stating it in this way. For example, on RHex there has been past work to push the body uphill and be centered over the legs while climbing steep terrain [4, 5],

[*] Electrical and Systems Engineering Department, University of Pennsylvania, 200 South 33rd Street, Philadelphia, PA 19104 {aaronjoh,kod}@seas.upenn.edu

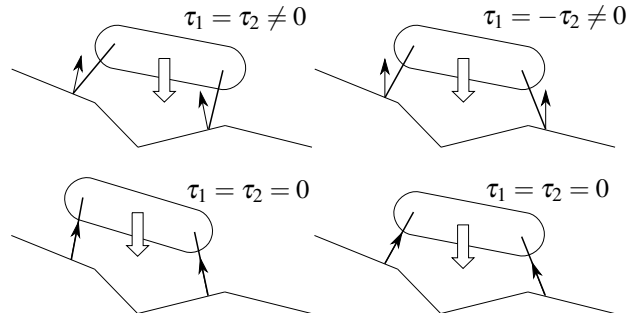[†] NREC, Carnegie Mellon University, Ten 40th St, Pittsburgh, PA 15201 gch@cs.cmu.edu

Fig. 1: Two examples of how the balancing stand works, noting the relationship between motor torques. On the left, start and end conditions for fighting an external force, on the right start and end conditions for relaxing an internal force.

as well as approaches that regulate individual leg torques such that no one leg pushes much harder than the rest [6]. These ideas were further developed by research on RiSE [7, 8] whose reactive gait phase adjustments were designed to balance forces within and between the sides with the goal of evenly distributing ground reaction forces. Prior work on a quadruped standing posture has been based on simultaneously trying to achieve multiple goals [9].

Why worry about the power used when the robot is idle? In one urban search and rescue study researchers discovered that for 49% of the robot's deployment it remained stationary, as the operators needed that time to gain situational awareness [10]. This corroborates our own experiences in a series of tests in the Mojave desert, where the robot was required to complete a course through a diversity of challenging terrain. In these tests the operator would often pause the robot in a standing posture while deciding how to proceed. In at least one specific instance during a trial in March of 2010, this caused a motor to burn out after less than a minute of standing. Robots operating on challenging terrain, especially in the heat of a desert, need a low-energy standing posture for health and mission runtime.

II. KINEMATICS OF A SELF-MANIPULATION

By *self-manipulation* we mean the process of using one's limbs to rearrange one's body (to follow the opening line of [11]) [12–14], broadly including any activity that alters a robot's configuration, whether or not it affects the center of mass frame. Figure 2 suggests how the self-manipulation problem we setup below relates to more traditional manipulation and locomotion problems. Joining these perspectives motivates our exploration of the long noted more general du-
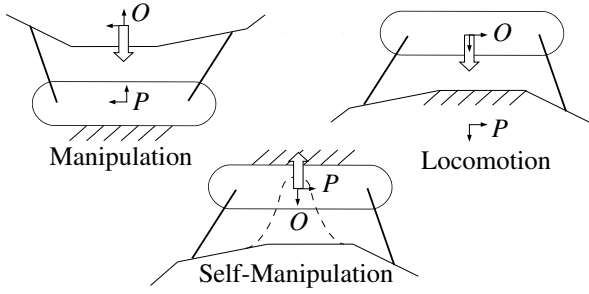
Fig. 2: Comparison of a traditional manipulation and locomotion problem formulations with the self-manipulation used in this paper. In each, P is fixed and O is not.

ality between locomotion and manipulation[1] [14–17], leading to dual-use actuators that can locomote and manipulate [18–23], as well as lending insight into locomotion through manipulation [17] or the reverse [24].

Following that tradition, this section presents a grasp-theoretic analysis of a two-stick-legged, standing planar robot with one motor at each hip[2]. Namely, following the methods developed in [2], we analyze the wrenches that act on the body using the grasp map to distinguish the internal and external forces applied to the body by the world, as the grasped object.

Table I and Figure 3 summarize the notation used in this paper, matching [2, Figures 5.14, 5.15], but relegate to the Appendix a more careful definition of some of these symbols.

A. Problem Setup

Let the inertial coordinate frame (origin or "palm" frame), P, as shown in Figure 3, be at the center of the robot. Let the moving object frame, O, be co-located at P initially, but connected to the ground. The standard problem formulation for a multi-finger grasp has a rigid "palm" and a movable "object." One normally treats the ground as rigid and the robot as movable, however considering the world from the robot's perspective it appears that the earth is attracted to the robot via gravity, and not the other way around. By co-locating the object and palm coordinate frames we can easily consider the wrenches and twists at that point of the world, and the robot's actual motion will simply be the opposite sign (from our ground based observation). This difference is illustrated in Figure 2.

In this paper we are trying to minimize the thermal cost needed to stand. For a static motor thermal cost is proportional to the square of current, hence it is best to minimize the instantaneous power, $I^2 R$. Since a motor's static

---

[1]E.g., "a different way to view a person walking on a globe is to say the person is manipulating the globe with his feet," [15].

[2]The ideas presented in this section can be readily extended to work on a saggital plane embedded in SE(3): there will simply be "extra zeros" padding the homogeneous matrices that are commonly used in the literature.

$\mathbf{A}_{ab} : T\mathscr{G}_a \to T\mathscr{G}_b$	Adjoint transformation from a to b
$\mathbf{B}_c := \pi^T$	Wrench basis at contact
$C_k \in \mathscr{G}_c$	Contact frames (body aligned)
$\mathscr{C} := \pi\mathscr{G}_{c_1} \times \pi\mathscr{G}_{c_2}$	Space of contact positions
$\mathbf{E} \in \mathbb{R}^{2x2}, \mathbf{e}_m^T, \mathbf{e}_d^T \in \mathbb{R}^{1x2}$	Change of basis to mean and difference
$\mathbf{f} \in T^*\mathscr{C}$	Contact wrench magnitudes
$\mathbf{F} \in T^*\mathscr{G}_o$	Generalized force (wrench)
$F_k \in \mathscr{G}_f$	Finger frames (leg aligned)
$\mathbf{g}_{ab} \in \mathscr{G}_a$	Rigid transformation from A to B
$\mathbf{G} : T^*\mathscr{C} \to T^*\mathscr{G}_o$	Grasp map
$\mathscr{G}_a := SE(2)$	Space of transformations in frame A
$\mathbf{h} : \mathscr{U} \to \Theta \times \mathscr{G}_o$	Kinematic function of θ_m
$\mathbf{H} : \mathscr{U} \to T\Theta \times T\mathscr{G}_o$	Jacobian function of θ_m
$\mathbf{J}_h : T\Theta \to T\mathscr{G}_o$	Hand Jacobian
$\mathbf{J}_{sf}^s : T\mathscr{S} \to T\mathscr{G}_c$	Finger Jacobians
$k, n \in \mathbb{R}^+$	Leg index and number of legs
$M_k \in \mathscr{G}_m$	Motor frames (leg aligned)
$O \in \mathscr{G}_o, P \in \mathscr{G}_p$	Object and palm frames (body aligned)
$S_k \in \mathscr{G}_s$	Leg attachment frames (body aligned)
$\mathscr{U} := [-30°, 30°] \in \mathbb{R}$	Range of angles considered
$\mathbf{V}_o \in T\mathscr{G}_o$	Generalized velocity (twist)
$\mathbf{x}_c \in \mathscr{C}$	Contact location in the contact basis
$(\alpha_k, \beta_k) \in \pi\mathscr{G}_p$	Toe location in palm frame
$\gamma_k \in \mathbb{R}^+$	Effective gear ratio
$\delta, \mu \in \mathbb{R}$	External and internal Lyapunov functions
$\eta : \mathscr{G}_p \to \mathbb{R}$	Height function
$\theta \in \Theta := \mathscr{U}^2$	Joint angle vector
$\theta_k \in \mathscr{U}$	Joint angles
$\kappa \in \mathbb{R}^+$	Controller constants
$\lambda \in \mathbb{R}$	Internal force magnitude
$\xi \in T\Theta$	Saturated desired joint velocity
$\pi : SE(2) \to \mathbb{R}^2$	Projection down to linear components
$\Pi : T^*\Theta \to \mathbb{R}^+$	Power cost function
$\ell_k, \rho_k \in \mathbb{R}^+$	Body and leg lengths
$\sigma : \mathbb{R} \to \mathbb{R}$	Saturation function
$\tau \in T^*\Theta$	Torque
$\phi \in \mathscr{U}$	Orientation
$\omega \in T\Theta$	Desired joint velocity

TABLE I: Symbols used in this paper.

torque is proportional to the current, a natural goal to set is,

$$\Pi := \frac{1}{2} \begin{bmatrix} \tau_1 & \tau_2 \end{bmatrix} \begin{bmatrix} \tau_1 \\ \tau_2 \end{bmatrix} = \begin{bmatrix} \tau_m & \tau_d \end{bmatrix} \begin{bmatrix} \tau_m \\ \tau_d \end{bmatrix}, \quad (1)$$

where τ_m is the mean torque and τ_d is the difference in torques, to be defined in (17). A key insight that emerges from the grasp analysis is to break apart the functional form of $\Pi = \mu(\tau_1, \tau_2) + \delta(\tau_1, \tau_2)$, where $\mu(\tau_1, \tau_2) := \tau_m^2$ and $\delta(\tau_1, \tau_2) := \tau_d^2$. Section II-E will show that μ captures the cost due to gravity while δ captures the cost due to internal forces. Section III re-introduces the leg torques as sensors capable of reading directly the algorithmically effective approximations to the gradients of μ and δ. In this section we derive these motor torques, (22-23), by first identifying the relevant infinitesimal relationships, applying the closed loop constraint that the object and toes must move together, and then calculating the internal and external toe force magnitudes, on which the motor torques are based.

For the standing behavior in this paper we choose to restrict the legs to be "under" the robot, $\theta_k \in \mathscr{U} := [-30°, 30°]$, i.e. we ignore the case that the robot is on an excessively steep slope, and cases where we are not near a "typical" standing posture ($\theta_k \approx 0$). We will also assume that the robot
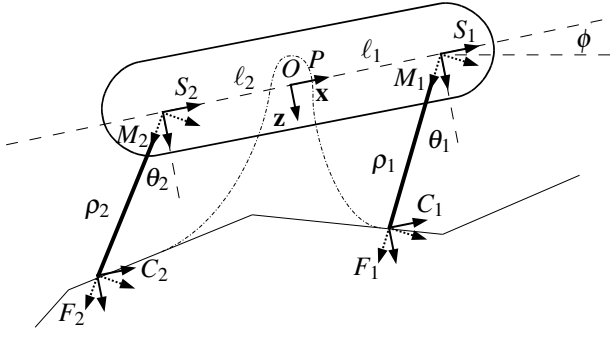
Fig. 3: Coordinate frames and key dimensions, with an object frame O connected to the ground but located at P. See Table I and the Appendix for details on these symbols (most of which we adopt from the manipulation literature [2, 25]).

is on terrain with sufficient friction and reasonable surface normals such that a balanced stand posture is with within the friction constraints[3]. This assumption is verified by the emperical results documented in Section IV.

B. Grasp Map and Hand Jacobian

The *wrench basis*, $\mathbf{B}_{c_i}$, at the contact points consists of the unit vectors of wrenches the toes can induce in the C_k frames ([2, Table 5.2], or [25, Table 2.3]). Here the toe can induce a $\mathbf{x}$ or $\mathbf{z}$ linear force but not a torque around $\mathbf{y}$. Thus $\mathbf{B}_{c_i}^T = \pi$, the projection down to only the linear components of the frame.

The *grasp map*, $\mathbf{G}$, takes wrenches at the projected contact points (i.e., forces at the toes), $\mathbf{f}_c \in T^*\mathscr{C}$ to wrenches on the object, $\mathbf{F}_o \in T^*\mathscr{G}_o$, and its dual, $\mathbf{G}^T$, acts covariantly, taking twists of the object, $\mathbf{V}_o \in T\mathscr{G}_o$, to twists at the contact point, $\dot{\mathbf{x}}_c \in T\mathscr{C}$, all expressed in coordinates as,

$$\mathbf{G}\mathbf{f}_c = \mathbf{F}_o \qquad \mathbf{G}^T\mathbf{V}_o = \dot{\mathbf{x}}_c \qquad (2)$$

[2, Equation 5.7, Figure 5.15], where here $\mathbf{G} \in \mathbb{R}^{3x4}$.

Next, the *hand Jacobian*, $\mathbf{J}_h$ relates infinitesimal motion at the joints, $\dot{\theta} \in T\Theta$ to twists at the contact points, $\dot{\mathbf{x}}_c \in T\mathscr{C}$, and has a dual, the pullback from toe forces, $\mathbf{f}_c \in T^*\mathscr{C}$ to hip torques, $\tau \in T^*\mathscr{C}$, all expressed as,

$$\mathbf{J}_h\dot{\theta} = \dot{\mathbf{x}}_c \qquad \mathbf{J}_h^T\mathbf{f}_c = \tau \qquad (3)$$

[2, Equations 5.16, Figure 5.15], where here $\mathbf{J}_h \in \mathbb{R}^{2x4}$. See the Appendix equations (37-40) for the explicit values of $\mathbf{B}_{c_i}$, $\mathbf{G}$, and $\mathbf{J}_h$, as well as a connection between $\mathbf{G}$ and $\mathbf{J}_h$ in equations (41-44) unique to self-manipulation (but not needed for this controller).

C. Forward Kinematics of the Closed Loop Constraint

The available free motion in stance is limited by the kinematic closed loop constraint, asserting that the toe contact frame, C_k, seen from the hip joints (rigidly attached to

---

[3]Note that this rules out any "jammed" postures — in such a case the robot would almost certainly need to know the surface normals and frictional coefficients, and then the controller could simply abide by the constraints in the typical manor [2, Sections 5.2-5.3].

the palm coordinate system) coincides with the toe contact frame seen from the object, which lifts to a tangent bundle constraint of the form,

$$\mathbf{J}_h\dot{\theta} = \mathbf{G}^T\mathbf{V}_o, \qquad (4)$$

[2, Equation 5.15], asserting that the motion of the contact frames as seen from the hand and the object agree.

Since the base space constraint is expressed as a difference in $\mathscr{C}$ over the images of a map on $\Theta \times \mathscr{G}_o$, its lift (4) imposes four linear constraints on five tangent vector components, necessitating a one dimensional null space in $T\Theta \times T\mathscr{G}_o$. The associated implicit function in the base space, $\Theta \times \mathscr{G}_o$, can be parametrized in many ways, but for present purposes it is convenient to choose the free variable to have a lift into the mean hip velocity, $\theta_m := \mathbf{e}_m^T\theta := \frac{1}{2}[1\ 1]\theta$. This choice is motivated by the observation that motion has equal cost in both motors, i.e. our total cost will be the sum of individual motor costs (incurred by the static torques they support). The associated implicit function on some open neighborhood of the origin, $\mathscr{U} \subset \mathbb{R}$,

$$\mathbf{h} : \mathscr{U} \to \Theta \times \mathscr{G}_o : \theta_m \to (\mathbf{h}_h(\theta_m), \mathbf{h}_o(\theta_m)) \qquad (5)$$

will be a local immersion — i.e., its Jacobian maps,

$$\mathbf{H}_h := D_{\theta_m}\mathbf{h}_h = \frac{2}{\gamma_1 + \gamma_2}\left[\begin{array}{c}\gamma_1 \\ \gamma_2\end{array}\right] \qquad (6)$$

$$\gamma_1 := (\ell_1 + \ell_2)\beta_2 + \rho_1\rho_2\sin(\theta_2 - \theta_1) \qquad (7)$$

$$\gamma_2 := (\ell_1 + \ell_2)\beta_1 + \rho_1\rho_2\sin(\theta_2 - \theta_1) \qquad (8)$$

$$\mathbf{H}_o := D_{\theta_m}\mathbf{h}_o = \qquad (9)$$

$$= -\frac{2\rho_1\rho_2}{\gamma_1 + \gamma_2}\left[\begin{array}{c}(\ell_1 + \ell_2)\cos\theta_1\cos\theta_2 \\ \ell_1\cos\theta_1\sin\theta_2 + \ell_2\cos\theta_2\sin\theta_1 \\ \sin(\theta_2 - \theta_1)\end{array}\right] \qquad (10)$$

(derived from (4)) will be full rank (never passing through the origin) in both tangent spaces (for $\theta_k \in \mathscr{U}$).

$\mathbf{H}_h$ (which can be thought of as the instantaneous gear ratios for two independent motor shafts coupled rigidly to a single external output load shaft) is nonsingular for $\theta_k \in \mathscr{U}$,

$$\gamma_1 \geq (\ell_1 + \ell_2)\rho_2\cos(-30) + \rho_1\rho_2\sin(-30 - 30) \qquad (11)$$

$$= \frac{\rho_2\sqrt{3}}{2}(\ell_1 + \ell_2 - \rho_1) > 0 \qquad (12)$$

and similarly for γ_2. In other words for at least the angular bounds of a standing posture, the robot will not reach a singularity in the closed chain kinematics.

If γ were known online we could scale the motion at each hip by its gear ratio to get the effective "output" motion produced by that motor, i.e. $\tilde{\theta}_m := \theta_1/\gamma_1 + \theta_2/\gamma_2$. This would have eliminated any coupled motion in the orthogonal direction, $\tilde{\theta}_d := \theta_1/\gamma_2 - \theta_2/\gamma_1$, as with our choice, $\partial\theta_d/\partial\theta_m = (\gamma_1 - \gamma_2)/(\gamma_1 + \gamma_2)$, but $\partial\tilde{\theta}_d/\partial\tilde{\theta}_m = 0$. However the robot will not have access to γ exactly due to contact ambiguity and compliance in the legs. Fortunately, for $\theta_k \in \mathscr{U}$, γ_1 and γ_2 are nearly identical. When the robot has equal length legs that are parallel, as is the nominal stance configuration, the two gear ratios are in fact equal, implying both that $\theta_m \equiv \tilde{\theta}_m$ and $\partial\theta_d/\partial\theta_m = 0$. Furthermore, for typical

values of ρ and ℓ, and with $\theta_k \in \mathscr{U}$, the gear ratios can be bounded numerically by $0.83 \leq \gamma_1/\gamma_2 \leq 1.19$.

D. Internal and External Forces at the Toes

The force due to the gravitational potential field, $\mathbf{F}_g$, is derived from the height $\eta : \mathscr{G}_p \to \mathbb{R}$ in that potential field and, at static equilibrium, it is exactly balanced by the contact forces,

$$\mathbf{G}\mathbf{f}_c = -\mathbf{F}_g; \quad \mathbf{F}_g := mgD\eta = \begin{bmatrix} mg\sin(\phi) \\ -mg\cos(\phi) \\ 0 \end{bmatrix} \quad (13)$$

whose "internal" component lies in the subspace [2, Definition 5.3],

$$\ker(\mathbf{G}) = \mathrm{Im}(\mathbf{f}_N) := \{\lambda\mathbf{f}_N | \lambda \in \mathbb{R}\}; \quad \mathbf{f}_N := \begin{bmatrix} \alpha_2 - \alpha_1 \\ \beta_2 - \beta_1 \\ \alpha_1 - \alpha_2 \\ \beta_1 - \beta_2 \end{bmatrix} \quad (14)$$

that will form our homogeneous solution, i.e. toe forces that are *internal* in that they can perform no work on the object.

To specify a particular solution, (13) must be augmented with an internal motor torque constraint of the form $\mathbf{e}_d^T \tau := \frac{1}{2}[1\ \text{-}1]\tau = 0$ imposed upon the hip joint torque vector, $\tau \in \mathbf{T}^*\Theta$, (3), just as a differential does in a car[4]. Pulling back through the infinitesimal kinematics (3), this now constrains the paired toe force magnitude vector $\mathbf{f}_c \in T^*\mathscr{C}$ leading to a unique solution of the full rank augmented version of (13) taking the form,

$$\mathbf{e}_d^T \mathbf{J}_h^T \mathbf{f}_c = 0; \quad \mathbf{f}_p := -\begin{bmatrix} \mathbf{G} \\ \mathbf{e}_d^T \mathbf{J}_h^T \end{bmatrix}^{-1} \begin{bmatrix} \mathbf{F}_g \\ 0 \end{bmatrix} \quad (15)$$

This choice of particular solution, depicted in the lower sketches of Figure 1, corresponds to toe forces that cancel gravity with the "right amount" of internal force, here defined by the difference condition. Observe that the homogeneous solution is then only the "extra" internal force. Thus the overall vector of paired toe force magnitudes is,

$$\mathbf{f}_c = \mathbf{f}_p + \lambda\mathbf{f}_N \quad (16)$$

E. Internal and External Torques at the Hips

The torque produced by these toe forces is given by the hand Jacobian, $\mathbf{J}_h^T$, as in (3). We will find it convenient to work in a new basis for the joint-space torques, $\tau \in \mathbf{T}^*\Theta$, given by the scaled rotation $\mathbf{E}$ into the mean and difference of the torques,

$$\begin{bmatrix} \tau_m \\ \tau_d \end{bmatrix} := \mathbf{E}\tau \qquad \mathbf{E} := \begin{bmatrix} \mathbf{e}_m^T \\ \mathbf{e}_d^T \end{bmatrix} = \frac{1}{2}\begin{bmatrix} 1 & 1 \\ 1 & -1 \end{bmatrix} \quad (17)$$

Here again if we wanted to look at the average output torque we would rotate not into $\mathbf{e}_m$ but into the "gear ratio" vector,

---

[4]One alternative is an internal force constraint $\mathbf{f}_N^T\mathbf{f}_c = 0$ [25], as in the upper right corner of Figure 1, however we allow some internal force to ensure no internal torque. Another alternative is to eliminate the difference in output torques, where $\mathbf{e}_d^T$ should be weighted by γ. However our cost is proportional to the unweighted sum of motor torque, $\tau^T\tau$.

$\mathbf{H}_h$. However, actual cost arises from motor torque, and so the torque implication of the particular solution ($\lambda = 0$) is,

$$\begin{bmatrix} \tau_m \\ \tau_d \end{bmatrix}_p := \mathbf{E}\mathbf{J}_h^T \mathbf{f}_p \quad (18)$$

$$= 2mg\rho_1\rho_2 \frac{\ell_1\cos\theta_1\sin(\theta_2\text{-}\phi) + \ell_2\cos\theta_2\sin(\theta_1\text{-}\phi)}{\gamma_1 + \gamma_2} \begin{bmatrix} 1 \\ 0 \end{bmatrix} \quad (19)$$

where $\tau_{d,p} = 0$ because the particular solution has no component in the $\mathbf{e}_d^T$ direction (15). Therefore all of the virtual work against gravity must show up in $\tau_{m,p}$, (note that $\mathbf{E} = \mathbf{E}^T = \mathbf{E}^{-1}/2$),

$$\mathbf{F}_g^T\mathbf{V}_o = \tau^T\dot{\theta} \quad (20)$$

$$\mathbf{F}_g^T\mathbf{H}_o\dot{\theta}_m = 2\tau^T\mathbf{E}^T\mathbf{E}\dot{\theta} = 2\tau_{m,p}\dot{\theta}_m \quad (21)$$

so that Equation 19 can be rewritten as,

$$\begin{bmatrix} \tau_m \\ \tau_d \end{bmatrix}_p = \frac{\mathbf{F}_g^T\mathbf{H}_o}{2}\begin{bmatrix} 1 \\ 0 \end{bmatrix} = \frac{mgD\eta \circ D\mathbf{h}_o}{2}\begin{bmatrix} 1 \\ 0 \end{bmatrix} \quad (22)$$

The torque projection of the homogeneous solution is,

$$\begin{bmatrix} \tau_m \\ \tau_d \end{bmatrix}_h := \lambda\mathbf{E}\mathbf{J}_h^T\mathbf{f}_N = \frac{\lambda}{2}\begin{bmatrix} \gamma_2 - \gamma_1 \\ \gamma_2 + \gamma_1 \end{bmatrix} \quad (23)$$

Here there is not an exact decomposition — we would like $\tau_{m,h}$ to be zero[5] so that τ_m is exactly $\tau_{m,p}$. However we have shown that $\gamma_1 \approx \gamma_2$, and in any case if our controller is successful we can achieve this by simply canceling the internal force magnitude, λ.

III. CONTROLLER DESIGN

In this section, we will use the infinitesimal kinematic analysis above to show how direct current readings at the hips yield intrinsic sensors that approximate the gradient of two costs, μ and δ, eliminating all need to know or compute any of $\mathbf{G}$, $\mathbf{J}_h^T$, $\mathbf{V}_o$, $\mathbf{F}_g$, $\mathbf{H}$, $\mathbf{f}_p$, $\mathbf{f}_N$, or even ℓ or ρ online. The change of basis in torque space, $\mathbf{E}$, allows the robot to use these sum and difference torque measurements to closely approximate the gradient of its power-use cost function.

A. Actuator Model

Because the motor controller is highly overdamped and rate limited we adopt "generalized damper" mechanics and model the motor as velocity controlled in general,

$$\dot{\theta} = \kappa_p\xi \quad (24)$$

for some command $\xi \in T\Theta$, however the motion is constrained by the closed loop condition (4), and so the constrained motion will be approximately,

$$\dot{\theta}_m = \kappa_p\xi_m \quad (25)$$
$$\dot{\theta}_d = 0 \quad (26)$$

Since the system can move freely in approximately the θ_m direction (exactly, in the $\mathbf{H}_h$ direction at any given

---

[5]And it fact it would be if we worked with the average output torque, $\tilde{\tau}_{m,h} = \gamma_1\gamma_2 - \gamma_2\gamma_1 = 0$.

θ_m), the motor generated torque must exactly balance the external (gravitational load torque), i.e. $\tau_{m,p} + \tau_{m.h}$ from (22), (23), by assumption of quasi-static operation. In contrast, in the approximate θ_d direction (exactly, along infinitesimal motions orthogonal to $\mathbf{H}_h$ for a specified θ_m), motion is locked, hence generated torque must increase as,

$$\dot{\tau}_d = k_t \xi_d \qquad (27)$$

i.e. any differentially applied command will increase the torque as the system cannot move in that direction. Again, we emphasize that this locked leg assumption is merely an approximation, but it will be a very good approximation when the shift in θ_d is slight ($\partial\theta_d/\partial\theta_m$ is small), as holds true in our setting. In truth no matter how large the shift, so long as $\gamma > 0$ for all angles, i.e. the sign of the direction of motion is correct, we can simply allow the internal force controller to compensate for this "disturbance" in θ_d as we move[6]. Moreover this misalignment between the approximate and true parameterization of the free motion does not affect the zero point — in either case the zero has $\tau_1 = \tau_2 = 0$ and so the controller will converge to the correct place, even if it does not take the "most direct" route.

To guarantee that the system remains quasi-static, we rate limit the control variable,

$$\xi_k = \sigma(\omega_k); \quad \sigma(\omega_k) := \begin{cases} \omega_k & |\omega_k| \le \kappa_\sigma \\ \operatorname{sign}[\omega_k]\kappa_\sigma & |\omega_k| > \kappa_\sigma \end{cases} \qquad (28)$$

and $\omega \in T\Theta$ is the desired velocity of the joint space variable, θ.

B. Internal Cost

We have shown in (22) that the particular solution (gravitational load with only the desired internal force) makes no contribution to τ_d, and, specifically, from (23), $\delta = \tau_d^2 = \lambda^2(\gamma_1 + \gamma_2)^2/4$ is the cost of the "extra" internal force. Moreover, since we have shown (12) that γ_k is bounded above zero, it is clear that the internal cost, δ, vanishes if and only if τ_d sets $\lambda = 0$. Based on our actuator model (27), τ_d is commanded entirely by choice of desired difference velocities, ω_d, which essentially selects the magnitude of internal force, λ^2. Under these assumptions, it is straightforward to reduce δ. Namely, if we assert the difference reference velocity control policy, $\omega_d := -\kappa_d\tau_d$, then we have,

$$\dot{\delta} = 2\tau_d\dot{\tau}_d = \begin{cases} -2\kappa_d\kappa_t\tau_d^2 & |\omega_d| \le \kappa_\sigma \\ -2\kappa_d\kappa_t\kappa_\sigma|\tau_d| & |\omega_d| > \kappa_\sigma \end{cases} \qquad (29)$$

so that the positive definite function, δ has a negative definite derivative along the motions of (27) with control specified as in (28), and, thus, as a Lyapunov function, assures that the approximate interntal torque, τ_d, decays to zero.

C. External Cost

We now address the second term of the cost function, $\mu = \tau_m^2$. Recall that $\tau_m^2 = (\tau_{m,p} + \tau_{m,h})^2$, and where,

$$\tau_{m,p} = mgD\eta_o(\theta_m); \quad \eta_o := \eta \circ h_o \qquad (30)$$

is determined by the gravitational torque field. It now follows that μ can be minimized asymptotically by minimizing the gravitational torque field magnitude. For this it suffices to bring θ_m to a critical point of η_o, and for $\phi \in \mathscr{U}$, the closest critical point is a local maximum[7]. Therefore, we will consider minimizing the function $-\eta_o$, and implement the quasi-static dynamics $\omega_m := \kappa_m\tau_m$, since this implies[8],

$$-\dot{\eta}_o = -D\eta_o \cdot \dot{\theta}_m = \begin{cases} -mg\kappa_m\kappa_p|D\eta_o|^2 & |\omega_m| \le \kappa_\sigma \\ -\kappa_p\kappa_\sigma|D\eta_o| & |\omega_m| > \kappa_\sigma \end{cases} \qquad (31)$$

i.e., $-\eta_0$ (a smooth positive definite function in the neighborhood of a maximum), has a negative definite derivative under the control input (28) as it enters the dynamics (25), and we immediately conclude that θ_m converges to its minimum, the local maximum of η_o, as desired.

D. Implementation on a Spatial Hexapod

We implement these ideas on the hexapod X-RHex by straightforward generalization of the difference torque controller (29), for each leg individually, and the mean torque controller (31), now applied to the mean of all six legs. Here, starting in this subsection, the space of configurations angles is $\theta \in \mathscr{U}^6$, the mean angle is still $\theta_m \in \mathscr{U}$, while there are now six difference angles, $\theta_d \in \mathscr{U}^6$, having the redundancy that $\sum_j \theta_{d,j} = 0$ (in the two legged version, there was $\tau_d = \tau_{d,1} = -\tau_{d,2}$). Each additional leg will add one more degree of freedom and two more constraints. In the rigid world of the previous section, the robot would only be able to move if all legs were parallel. In the physical hexapedal implementation, the compliance of the legs provides additional degrees of freedom, and furthermore the robot is allowed to break some constraints when a leg loses contact with the ground. In general, with even more legs, the chance of some redundant legs lifting off the ground is even higher, although we expect the controller will still work.

The reactive stand is initiated with a traditional open loop stand behavior, and then the following controller is applied based on the leg torques, τ, as follows,

$$\omega_m = \kappa_p \frac{1}{n}\sum_{j=1}^{n}\tau_j = \kappa_m\tau_m \qquad (32)$$

$$\omega_{d,k} = -\kappa_d\left(\tau_k - \frac{1}{n-1}\sum_{j \ne k}\tau_j\right) = -\kappa_d\tau_{d,k} \qquad (33)$$

$$\omega_k = \omega_m + \omega_k \qquad (34)$$

where n is the number of legs (2 in the simple case of the previous section, 6 in the full case)[9]. This very directly encodes the notion of fighting the mean (sum of all legs), and canceling the difference (between one leg and the normalized sum of the rest).

---

[6]Without this dependence, the two controllers could be run sequentially.

[7]Naturally the configuration of the robot at the critical point based on any non-singular parameterization will be the same as it is really a critical point of the true potential, η.

[8]The coupling of $\tau_{m,h}$ will add a sign indefinite term to the top line, $-\lambda\kappa_m\kappa_p\frac{\gamma_2-\gamma_1}{2}D\eta_o$, but λ is exponentially driven to zero by (29).

[9]Note that equivalently we can set $\dot{\omega}_{d,k} = -\tilde{\kappa}_{d,k} \cdot \tau_k$ while making $\dot{\omega}_m = \tilde{\kappa}_m\sum_j \tau_j$ by changing our gains appropriately.

Fig. 4: X-RHex performing a reactive stand on rocks

IV. EXPERIMENTAL RESULTS

A. Reactive Standing

This self-manipulation controller was first tested on a variety of outdoor terrains. The robot starts from a seated position on the ground where the idle "hotel" power is measured (about 29.1 W for these trials), and then it performs a normal stand followed by a reactive stand. Figure 4 shows a test on a pile of rocks, and Table II summarizes the results. Each row is an average over five trials, and the power measurements have the "hotel" load removed (as we are not concerned with reducing the power used by the onboard computer or other electronics).

Terrain	Slope	Normal Power	Reactive Power	Change
Asphalt	None	6.02 W	3.64 W	39.6%
Rocks	Various	6.32 W	3.73 W	40.1%
Grass	-14.0° pitch, 11.1° roll	5.89 W	4.12 W	30.0%
Grass	1.2° pitch, 5.5° roll	11.43 W	4.34 W	62.0%
Dirt	18.8-19.9° pitch	22.50 W	4.01 W	82.2%

TABLE II: Reactive stand power from seated position. Each row is an average of five trials.

Note that regardless of the starting power, the reactive power was reduced to around 4 W. In fact the maximum reactive power use over all 25 trials was only 4.97 W. Anecdotally, usually the entire robot can be turned off and the robot will remain standing (implying that the remaining 4 W mostly came from the control electronics or noise).

A second set of experiments was conducted starting from a walking gait on various terrains, as is summarized in Table III. Again, a total of five experiments per terrain were averaged. Every trial except for one on the rubble pile reduced the power to around 4 W. In that outlier, with a final power usage of 21.2 W, the robot slipped partway through execution of the smart stand, and, as the current behavior executes for a fixed time, the robot did not have time to completely recover. While simple modifications could alleviate this (such as executing the behavior a second time), it brings up the issue that the current behavior does not know

the friction constraints of the surface and has no means of reacting to events such as slipping.

Terrain	Slope	Normal Power	Reactive Power	Change
Carpet	None	36.63 W	3.97 W	89.2%
Smooth Surface	10.6° pitch	15.55 W	3.98 W	74.4%
Rubble Pile	Various	31.25 W	7.30 W	76.62%

TABLE III: Reactive stand power from a walking behavior. Each row is an average of five trials.

B. Reactive Walking

Extrapolating these ideas into a walking task introduces a variety of new issues and we only briefly sketch our preliminary adaptations and experiments as motivation for future work. A full extension to a walking controller will have to consider the problem of providing enough propulsive power while ascending slopes [4, 5], and problem of "combinatorial obstacles" [26] required to maintain enough legs on the ground at all times. Thus a full walking version of this controller is outside the scope of this paper.

However this initial walking behavior implements the leg variance strategy of balancing internal differences throughout the stance (akin to [7]). Thus the walking controller cannot reduce the power draw to zero (as the robot must keep moving) but instead can only redistribute which legs are providing torque, allowing legs to adapt to the terrain and provide a more even footing. This will also reduce the thermal cost of locomotion.

The walking controller runs a normal gait [1], but adjusts the per leg phase offset, ϕ_0 from that paper,

$$\dot{\phi}_{0,k} = -\kappa_d \cdot \left(\tau_k - \frac{\sum_j \tau_j}{2n_s} \right) \qquad (35)$$

where n_s is the number of legs in contact on leg k's side, while the sum goes over all legs. In this way the controller tries to balance the torques within and between the sides.

The reactive walking behavior was tested over a fixed distance with a single, 9.2 cm high cinder block, that is just shorter than the body clearance height. The robot was lined up so that only the left side would hit the obstacle. The results (Table IV) are an average over ten trials, while the total energy has the "hotel" load (about 21.1 W for these trials) removed. The second set of trials includes a 5 kg payload mass.

The reactive walking behavior did cause a small increase in overall energy used, most likely due to the effective softening of each leg. However the leg with the highest thermal cost in a given trial (typically the front left leg in this case) saw a significant reduction in that thermal cost — a not infrequent cause of robot failure, particularly in hot environments like the Mojave Desert mentioned in the Introduction. Thus the thermal cost has been more evenly shared among the available motors.

Method	Robot Mass	Trial Time	Total Energy	Thermal Energy	Peak Leg Thermal
Normal	9 kg	4.79 s	94.58 J	45.73 J	19.24 J
Reactive	9 kg	4.99 s	97.81 J	43.02 J	12.16 J
Improvement	-	-4.2%	-3.4%	5.9%	36.8%
Normal	14 kg	5.64 s	143.0 J	90.11 J	34.69 J
Reactive	14 kg	5.61 s	148.4 J	80.87 J	22.57 J
Improvement	-	1.9%	-6.0%	6.4%	30.0%

TABLE IV: Reactive walking results over a fixed distance with a single obstacle. Each row is an average of 10 trials.

V. CONCLUSION

We have demonstrated a quasi-static self-manipulation behavior on RHex that dramatically reduces energetic and thermal costs by servoing on simple sums and differences of actuator currents. We derive these strategies by consideration of the relationships between internal and external work applied to the joints by the actuators and by gravity. The key insight entails a change of basis in the robot's joint space that approximates the intrinsically decoupled nature of the two types of forces, establishing the correspondence of these sums and differences of currents to gradients of the very cost functions whose minimization is sought, all without having to carefully model the system online.

The correctness of this controller could have been shown using first principles kinematics and geometry, however we chose to model the robot as if it were a multi-fingered hand. This allowed us to leverage the insight developed over decades of research in that field, leading to very simple expressions of the toe/ground interaction, the closed chain constraint, and the internal forces. As this was a self-manipulation, we were able to co-locate the palm and object frames to allow the usual assumption of a fixed palm and moving object, but still calculate forces and motions at that location. This self-manipulation analysis was only needed here to verify the correctness of the simple controller, however it will allow us to leverage further results from manipulation as our robots continue to use their legs more like fingers and think more carefully about how they are grasping the ground.

ACKNOWLEDGMENTS

APPENDIX

This appendix provides more detailed explanations of notation, full matrix values, and explores a relationship between $\mathbf{J}_h$ and $\mathbf{G}$ unique to self-manipulation.

Denote a rigid frame B, expressed in the coordinates of rigid frame A (or, equivalently, a rigid transformation that takes frame A into frame B) $\mathbf{g}_{ab} \in \mathscr{G}_a := SE(2)$, while an adjoint transformation matrix, $\mathbf{A}_{ab} : T\mathscr{G}_a \to T\mathscr{G}_b$ as a shorthand for $\mathbf{Ad}_{\mathbf{g}_{ab}}$, maps body velocity in twist coordinates to spatial velocity in twist coordinates [2, Sections 2.3-2.4]. Working in the saggital plane, SE(2), we drop the out-of-plane direction (and associated roll or yaw angles) to write the coordinates of a frame as $\mathbf{g} = (x, z, \phi) \in \mathscr{G}$. We will need to model forces at pinned toe joints, hence denoting by π the projection from SE(2) to $\mathbb{R}^2$, we will express the origin of a frame, $\mathbf{g}$, as $\mathbf{p} = (x, z) = \pi\mathbf{g} \in \pi\mathscr{G} \approx \mathbb{R}^2$. The twist (tangent), $\mathbf{V} \in T_{\mathbf{g}}\mathscr{G}$ and wrench (cotangent) $\mathbf{F} \in T_{\mathbf{g}}^*\mathscr{G}$ spaces over a rigid frame, $\mathbf{g} \in \mathscr{G}$ necessarily figure prominently.

Define the following coordinate frames, as shown in Figure 3 (and corresponding to [2, Figure 5.14]). Let the inertial frame (origin or "palm" frame), P, be at the center of the robot, with the $+\mathbf{x}$ axis aligned with the robot, $+\mathbf{z}$ in the "downward" direction from the robot, and thus $+\mathbf{y}$ exiting the page (this is a standard "North, East, Down" orientation). As noted before, let the object frame, O, be co-located at P.

Define a frame fixed on the robot body, S_k, where each leg k attaches, and a rotating frame that moves with the motor, M_k, at the same point. At the end of the leg define a "finger" frame, F_k, pointing in the same direction. Hip 1 is located ℓ_1 away from the origin and the leg length is ρ_1, thus the leg 1 toe position in the palm frame is $(\alpha_1, \beta_1) := (\ell_1 - \rho_1 \sin\theta_1, \rho_1 \cos\theta_1)$, and the leg 2 toe position is $(\alpha_2, \beta_2) := (-\ell_2 - \rho_2 \sin\theta_2, \rho_2 \cos\theta_2)$.

The robot orientation relative to gravity is captured by the pitch ϕ, with $\phi = 0$ when the robot is horizontal and a positive pitch when hip 1 is higher than hip 2. The leg angles are measured as θ_1 and θ_2 in the clockwise direction from the body $+\mathbf{z}$ direction. All angles in Figure 3 are positive, and recall that we constrain $\theta_k \in \mathscr{U} := [-30°, 30°]$.

The contact frame, C_k, at each toe would typically be defined with the $\mathbf{z}$ axis pointing into the object, however we will not in general know the contact normals. So for convenience we will initialize it to be oriented in the same way as the robot body (i.e. we will assume the ground is parallel to the robot). Recall that for this paper we assume that the robot is on terrain with sufficient friction and reasonable surface normals.

The standard grasping analysis focuses on the collected directions of contact wrenches, in our case the collected linear components of the two contact frames,

$$(\mathbf{x}_{c_1}, \mathbf{x}_{c_2}) = \mathbf{x}_c \in \mathscr{C} := \pi\mathscr{G}_{c_1} \times \pi\mathscr{G}_{c_2} \approx \mathbb{R}^4 \qquad (36)$$

Rolling contact at RHex's toes yields the wrench basis,

$$\mathbf{B}_{c_i} := \begin{bmatrix} 1 & 0 \\ 0 & 1 \\ 0 & 0 \end{bmatrix}. \qquad (37)$$

The *grasp map* (2), $\mathbf{G} \in \mathbb{R}^{3x4}$ — the pullback over the (paired) rigid transformations from object frame, $\mathscr{G}_o$ to the (two) contact points, $\mathscr{C}$ — is defined as, [2, Equation 5.6],

$$\mathbf{G} := \begin{bmatrix} \mathbf{A}_{co_1}^T \mathbf{B}_{c_1} & \mathbf{A}_{co_2}^T \mathbf{B}_{c_2} \end{bmatrix} = \begin{bmatrix} 1 & 0 & 1 & 0 \\ 0 & 1 & 0 & 1 \\ \beta_1 & \text{-}\alpha_1 & \beta_2 & \text{-}\alpha_2 \end{bmatrix} \tag{38}$$

The *hand Jacobian* (3), $\mathbf{J}_h \in \mathbb{R}^{2x4}$ — the tangent lift of the kinematic map from joints, Θ, to paired toe positions, $\mathscr{C}$ — is defined as, [2, Equations 5.14],

$$\mathbf{J}_h := \begin{bmatrix} \mathbf{B}_{c_1}^T \mathbf{A}_{sc_1}^{-1} \mathbf{J}_{sf_1}^s & 0 \\ 0 & \mathbf{B}_{c_2}^T \mathbf{A}_{sc_2}^{-1} \mathbf{J}_{sf_2}^s \end{bmatrix} \tag{39}$$

$$= \begin{bmatrix} -\rho_1 \cos\theta_1 & -\rho_1 \sin\theta_1 & 0 & 0 \\ 0 & 0 & -\rho_2 \cos\theta_2 & -\rho_2 \sin\theta_2 \end{bmatrix}^T \tag{40}$$

Now consider the relation between $\mathbf{J}_h$ and $\mathbf{G}$. For traditional manipulations, these maps must be computed separately. In self-manipulation the object being manipulated is the manipulator itself, and so here we derive a common structure relating these Jacobians. While this relationship is unique to self-manipulations, and is computationally simpler than computing both Jacobians directly, neither is needed to complete this behavior, and so we leave the derivation of this connection in this Appendix as an interesting, but not necessary, analysis.

The two Jacobians can be written down as (with $\mathbf{d}_k$ is the axis of rotation for the kth leg, here $\mathbf{d}_k = -\mathbf{y}$),

$$\mathbf{G} = \begin{bmatrix} \mathbf{I} & \mathbf{I} \end{bmatrix} \begin{bmatrix} \mathbf{A}_{co_1}^T \mathbf{B}_{c_1} & 0 \\ 0 & \mathbf{A}_{co_2}^T \mathbf{B}_{c_2} \end{bmatrix} \tag{41}$$

$$\mathbf{J}_h^T = \begin{bmatrix} \mathbf{d}_1 \mathbf{A}_{pm_1}^T & 0 \\ 0 & \mathbf{d}_2 \mathbf{A}_{pm_2}^T \end{bmatrix} \begin{bmatrix} \mathbf{A}_{co_1}^T \mathbf{B}_{c_1} & 0 \\ 0 & \mathbf{A}_{co_2}^T \mathbf{B}_{c_2} \end{bmatrix} \tag{42}$$

The closed loop constraint equation (4) can then be written,

$$\begin{bmatrix} \mathbf{B}_{c_1}^T \mathbf{A}_{oc_1} & 0 \\ 0 & \mathbf{B}_{c_2}^T \mathbf{A}_{oc_2} \end{bmatrix} \begin{bmatrix} \mathbf{I} & \text{-}\mathbf{A}_{pm_1}\mathbf{d}_1^T & 0 \\ \mathbf{I} & 0 & \text{-}\mathbf{A}_{pm_2}\mathbf{d}_2^T \end{bmatrix} \begin{bmatrix} \mathbf{V}_o \\ \dot{\theta} \end{bmatrix} = \mathbf{0} \tag{43}$$

And the particular solution, $\mathbf{f}_p$ (15), will be,

$$\left(\begin{bmatrix} \mathbf{I} & \mathbf{I} \\ \mathbf{d}_1 \mathbf{A}_{pm_1}^T & \text{-}\mathbf{d}_2 \mathbf{A}_{pm_2}^T \end{bmatrix} \begin{bmatrix} \mathbf{A}_{co_1}^T \mathbf{B}_{c_1} & 0 \\ 0 & \mathbf{A}_{co_2}^T \mathbf{B}_{c_2} \end{bmatrix} \right)^{-1} \begin{bmatrix} \mathbf{w_g} \\ 0 \end{bmatrix} = \mathbf{f}_p \tag{44}$$

References

[1] U. Saranli, M. Buehler, and D. E. Koditschek, "RHex: A Simple and Highly Mobile Hexapod Robot," *The International Journal of Robotics Research*, vol. 20, no. 7, pp. 616–631, 2001.

[2] R. M. Murray, Z. Li, and S. S. Sastry, *A Mathematical Introduction to Robotic Manipulation*. Boca Raton, FL: CRC Press, 1994.

[3] K. C. Galloway, G. C. Haynes, B. D. Ilhan, A. M. Johnson, R. Knopf, G. Lynch, B. Plotnick, M. White, and D. E. Koditschek, "X-RHex: A highly mobile hexapedal robot for sensorimotor tasks," University of Pennsylvania, Tech. Rep., 2010.

[4] H. Komsuoglu, D. McMordie, U. Saranli, N. Moore, M. Buehler, and D. E. Koditschek, "Proprioception based behavioral advances in a hexapod robot," in *Robotics and Automation. Proceedings of the IEEE International Conference on*, vol. 4, 2001.

[5] G. C. Haynes and D. E. Koditschek, "On the comparative analysis of locomotory systems with vertical travel," in *International Symposium on Experimental Robotics*, Delhi, India, December 2010.

[6] J. D. Weingarten, R. E. Groff, and D. E. Koditschek, "A framework for the coordination of legged robot gaits," in *The IEEE International Conference on Robotics and Automation*, 2004, pp. 679–686.

[7] G. C. Haynes and A. A. Rizzi, "Gait regulation and feedback on a robotic climbing hexapod," in *Proceedings of Robotics: Science and Systems*, Philadelphia, USA, August 2006.

[8] G. C. Haynes, "Gait regulation control techniques for robust legged locomotion," Ph.D. dissertation, Robotics Institute, Carnegie Mellon University, Pittsburgh, PA, May 2008.

[9] J. Sousa, V. Matos, and C. Peixoto dos Santos, "A bio-inspired postural control for a quadruped robot: An attractor-based dynamics," in *Intelligent Robots and Systems (IROS), 2010 IEEE/RSJ International Conference on*, Oct. 2010, pp. 5329 –5334.

[10] J. Burke, R. Murphy, M. Coovert, and D. Riddle, "Moonlight in miami: Field study of human-robot interaction in the context of an urban search and rescue disaster response training exercise," *Human–Computer Interaction*, vol. 19, no. 1-2, pp. 85–116, 2004.

[11] M. T. Mason, *Mechanics of Robotic Manipulation*. Cambridge, MA: MIT Press, August 2001.

[12] H. Komsuoglu, "Dynamic legged mobility—an overview," in *Proceedings of International Joint Robotics Conference and Workshop*, 2009.

[13] U. Saranli, A. A. Rizzi, and D. E. Koditschek, "Model-based dynamic self-righting maneuvers for a hexapedal robot," *The International Journal of Robotics Research*, vol. 23, no. 9, pp. 903–918, 2004.

[14] K. Lynch, "Nonprehensile robotic manipulation: Controlability and planning," Ph.D. dissertation, Robotics Institute, Carnegie Mellon University, Pittsburgh, PA, March 1996.

[15] M. Yim, "Why study statically stable locomotion?" available online: http://robotics.stanford.edu/users/mark/loco-loco.html.

[16] M. Yim, J. Reich, and A. A. Berlin, *Distributed Manipulation*. Kluwer Academic Publishers, 2000, ch. Two approaches to distributed manipulation.

[17] B. Beigzadeh, M. N. Ahmadabadi, A. Meghdari, and A. Akbarimajd, "A dynamic object manipulation approach to dynamic biped locomotion," *Robotics and Autonomous Systems*, vol. 56, no. 7, pp. 570 –582, 2008.

[18] M. T. Mason, D. Pai, D. Rus, L. R. Taylor, and M. Erdmann, "A mobile manipulator," in *IEEE International Conference on Robotics and Automation (ICRA '99)*, vol. 3, May 1999, pp. 2322 – 2327.

[19] M. T. Mason, D. Pai, D. Rus, J. Howell, L. R. Taylor, and M. Erdmann, "Experiments with desktop mobile manipulators," in *International Symposium on Experimental Robotics*, 1999.

[20] S. Srinivasa, C. R. Baker , E. Sacks, G. Reshko, M. T. Mason, and M. Erdmann, "Experiments with nonholonomic manipulation," in *Proceedings of the IEEE International Conference on Robotics and Automation (ICRA)*, vol. 2. IEEE, May 2002, pp. 2042 – 2047.

[21] P. Ben-Tzvi, A. A. Goldenberg, and J. W. Zu, "Design and analysis of a hybrid mobile robot mechanism with compounded locomotion and manipulation capability," *Journal of Mechanical Design*, vol. 130, no. 7, p. 072302, 2008.

[22] Y. Liu and G. Liu, "Mobile manipulation using tracks of a tracked mobile robot," in *Intelligent Robots and Systems, IEEE/RSJ International Conference on*, Oct. 2009, pp. 948 –953.

[23] R. Voyles and A. Larson, "Terminatorbot: a novel robot with dual-use mechanism for locomotion and manipulation," *Mechatronics, IEEE/ASME Transactions on*, vol. 10, no. 1, pp. 17 –25, Feb. 2005.

[24] J. Hong, G. Lafferriere, B. Mishra, and X. Tan, "Fine manipulation with multifinger hands," in *The IEEE International Conference on Robotics and Automation*, May 1990, pp. 1568 –1573 vol.3.

[25] M. T. Mason and J. J. Kenneth Salisbury, *Robot Hands and the Mechanics of Manipulation*. Cambridge, MA: MIT Press, 1985.

[26] G. Haynes, F. Cohen, and D. Koditschek, "Gait transitions for quasi-static hexapedal locomotion on level ground," *Robotics Research*, pp. 105–121, 2011.